"Rapid tooling: investigation of soft-tooled micro-injection moulding process characteristics using in-line measurements and surface metrology",

Gülçür, M., Couling, K., Goodship, V., Charmet, J. and Gibbons, G.J. (2023),

ABSTRACT

Purpose – The objective of this research is to demonstrate and characterise a soft-tooled micro-injection moulding process through in-line measurements and surface metrology using a data-intensive approach.

Design/methodology/approach – A soft-tool for a demonstrator product that mimics the main features of miniature components in medical devices and microsystem components has been designed and fabricated using material jetting technique. The soft-tool was then integrated into a mould assembly on the micro-injection moulding machine and mouldings were made. Sensor and data acquisition devices including thermal imaging and injection pressure sensing have been set up to collect data for each of the prototypes. Off-line dimensional characterisation of the parts and the soft-tool have also been carried out to quantify the prototype quality and dimensional changes on the soft-tool after the manufacturing cycles.

Findings –The data collection and analysis methods presented here enable the evaluation of the quality of the moulded parts in real-time from in-line measurements. Importantly, it is demonstrated that soft-tool surface temperature difference values can be used as reliable indicators for moulding quality. Reduction in the total volume of the soft-tool moulding cavity was detected and quantified up to 100 cycles. Data collected from in-line monitoring was also used for filling assessment of the soft-tool moulding cavity, providing about 90% accuracy in filling prediction with relatively modest sensors and monitoring technologies.

Originality/value – The work presents a data-intensive approach for the characterisation of soft-tooled micro-injection moulding processes for the first time. The overall results show that the product-focussed data-rich approach presented here proved to be an essential and useful way of exploiting additive manufacturing technologies for soft-tooled rapid prototyping and New Product Introduction.

Keywords: rapid prototyping, rapid tooling, injection moulding, micro-injection moulding, 3D printing, data acquisition, thermal imaging, process monitoring, smart manufacturing, Industry 4.0

ABBREVIATIONS

AM	: Additive manufacturing
NPI	: New Product Introduction
μ-IM	: Micro-injection moulding
HDT	: Heat deflection temperature
T_g	: Glass transition temperature
PP	: Polypropylene
POI	: Point of interest
h_p	: Protrusion height
T_{sprue}	: Maximum temperature measured on the sprue
T_{max}	: Maximum temperature measured on the soft-tool
T_{max-c}	: Maximum temperature measured on the micro-featured cavity
A_p	: Pressure integral or area
A_{dev}	: Areal deviation near the gate
PID	: Proportional, integral, and derivative
R^2	: R-squared or coefficient of determination
S/O	: Switch-over
G'	: Storage modulus
G''	: Loss modulus
Δh_p	: Deviation from initial micro-feature replication
ΔT	: Temperature deviation
ΔT_{sprue}	: Temperature deviation in T_{sprue}
ΔT_{max}	: Temperature deviation in T_{max}
ΔT_{max-c}	: Temperature deviation in T_{max-c}
T_c	: Critical temperature
ROC	: Receiver operation characteristic

Introduction

Additive manufacturing (AM) has now become an indispensable stage of New Product Introduction (NPI), used where 3D models can be prototyped and visualised before mass production. This is a significant advantage as the product design can be modified to the consumer and market needs during the product development stage. However, the majority of mechanical, medical, and optical components are still being manufactured by replication and injection moulding processes that enable the use of application-specific materials and convenience in upscaling (Bibber, 2012; Peixoto *et al.*, 2022). This is done through labour-intensive and expensive mould tools that require significant investments. The high-costs of mould making is a result of advanced machining and/or milling processes of metals, all of which are subtractive and extremely specialised processes (Holthusen *et al.*, 2017; Gülçür *et al.*, 2021; Boinski *et al.*, 2022); making any modifications needed on the mould tools expensive and time consuming. Thus, a lot of time and effort should be expended during the product and tool design phases to make any investment in the tooling viable. In this context, mould tools or micromoulding inserts can be manufactured using AM with soft materials for prototyping or low-volume manufacture purposes (Harris *et al.*, 2003; Bagalkot *et al.*, 2019; Zhang *et al.*, 2017). Such soft-tools enable the manufacture of moulded prototypes without prohibitive commitments and investments inherent to conventional mould tool procurement. Hence, additively manufactured injection mould tools or soft-tool inserts have the potential to provide significant advantages for optimising rapid product design and prototyping before or during NPI (Williams and Kochhar, 2000).

The utmost need for rapid and responsive manufacturing is being witnessed in various areas with the advancements in micro-and-nano technologies, the most prominent example being the medical sector, as the COVID19 pandemic also has recently shown (Xu *et al.*, 2021; Ayylidiz *et al.*, 2020; *University of Bradford begins mass production of face shields for health service,*

2020). In such a state of emergency, various components had to be designed and manufactured in the shortest time possible in a cost-effective manner. AM or soft-tooled injection moulding processes have been used to manufacture ventilator components, face shields and test swabs during the pandemic (Ayylldlz *et al.*, 2020; *University of Bradford begins mass production of face shields for health service*, 2020; *Ventilators, visors, volunteers and testing - more than a dozen more ways Warwick staff & students are helping respond to the pandemic*, 2020). Yet, the soft-tooled injection moulding process is still in its infancy, and there are potentials to exploit its capability for delivering even higher quality prototypes and products. Soft-tooled moulding processes are significantly different from the conventional approach, where unique thermo-mechanical and dynamic aspects in the polymer tools bring unknown and unpredictable consequences regarding product quality and assessment (Kovács *et al.*, 2015; Mendible *et al.*, 2022). Recent advances in miniaturisation and technological improvements in AM are also very significant, as the techniques will be able to make soft-tools with ever smaller features and tighter tolerances (Zhu *et al.*, 2022). Hence, it is anticipated that functional microsystem devices will be made, assembled, and tested before NPI through soft-tooled rapid prototyping and moulding processes.

The advancements and developments towards miniaturisation in AM also overlap with the trends in the highly capable and established manufacturing technique known as micro-injection moulding (μ-IM) (Bibber, 2014; Bibber, 2012; Whiteside *et al.*, 2003; Gülçür and Whiteside, 2021). The technique has been the state-of-the-art for high-volume and economical manufacture of miniature medical devices, optoelectronics, and micromechanical components (Gülçür *et al.*, 2021; Romano *et al.*, 2019; Baruffi, Calaon and Tosello, 2018; Zhang *et al.*, 2021). Such capability also comes at the expense of very-high tooling costs, sometimes even higher than the cost of the manufacturing equipment itself (Formlabs, 2022). In this context, soft-micro-tools or inserts can be very effective for rapid prototyping in small volumes, even

though they might last for only a few prototypes (Zhang *et al.*, 2017; Krizsma *et al.*, 2021; Kovács *et al.*, 2015).

Current limitations in AM and limited understanding of the soft-tooled moulding processes make rapid prototyping in high-resolutions and with tighter tolerances challenging. Even though a number of micro-components can be fabricated using soft-tooling, their production cannot be reliably assured without process characterisation as shown herein. High-resolution AM of soft-tools is challenging because of the minimum feature size that can be achieved and mould-feature deformation during micromoulding (Bagalkot *et al.*, 2019; Gohn *et al.*, 2022). Hence, characterisation and development of rapid, soft-tooled μ-IM processes are essential for delivery and development of high-added value products in significantly reduced time frames. Some of the significant technical challenges and areas that require improvements in soft-tooling for μ-IM can be summarised as below:

- Characterisation of process dynamics; e.g. injection, filling, ejection, clamping (Whiteside *et al.*, 2005),

- Heat transfer and temperature control of the soft-tools or inserts (Kovács *et al.*, 2015),

- Soft-tool durability or lifespan (Zhang *et al.*, 2017),

- Limitations in the printing resolution (Dilag *et al.*, 2019; Yang *et al.*, 2017).

There are few reported research articles using in-line monitoring of soft-tooled μ-IM processes. Moreover, no publications were found utilising multi-channelled process data acquisitions for the characterisation of soft-tools. One of the earlier works Harris et.al presented temperature measurements near the cavity surface of soft-tools made using stereolithography (Harris *et al.*, 2003). The authors used the temperature data acquired by k-type thermocouples for shrinkage evaluation of the parts. They reported that shrinkage of amorphous polymers was unaffected due to mould material type which makes them preferable for soft-tooled prototyping applications. Another study from the same authors focussed on the evaluation of ejection forces

via in-line collected data through a strain gauge attached to the back of the ejector pins in the mould assembly (Harris, Newlyn and Dickens, 2002). It was emphasised that adhesion forces between the moulds manufactured using stereolithography and the parts can cause tool failure and ejection forces were evaluated for several thermoplastic materials. A mathematical model was also presented for prediction of ejection forces when using different moulding materials. Krizsma et. al carried out work on the in-situ monitoring of the deformation in soft-tools for injection moulding through mould-integrated strain gauges (Krizsma *et al.*, 2021). The authors reported significant correlations between cavity pressure measurements and strain gauge acquisitions which could be a cost-effective alternative for monitoring soft-tool condition and moulding process. Another recent work focussed on vision-based in-line monitoring of a soft-tooled injection moulding process where an optical and a thermal camera was used for dimensional quality prediction of the parts (Zhang *et al.*, 2022). A neural network was established for the estimation of the moulded parts, which is thought to be used as a compensation method for the machine control for obtaining defect-free parts. Although these reports prove to be invaluable when characterising a soft-tooled μ-IM process and make excellent contributions to the literature, there is still a need to implement further in-line measurement methods for processes in the μ-IM regimes. The in-line monitoring aspect of conventional μ-IM is a prominently researched area due to challenging process environments and miniature products (Whiteside *et al.*, 2004; Whiteside *et al.*, 2005; Gülçür and Whiteside, 2021; Santoso *et al.*, 2022; Zhang *et al.*, 2021; Gulcur, 2019). A majority of the similarities in the process can be exploited to characterise soft-tooled processes.

This work aims to tackle the above challenges and exploit the unique capability of rapid, soft-tooling described above by implementing in-line measurements for soft-tooled μ-IM process characterisation. The product designed in the current study is a sub-gram test component containing microstructures that mimic mould features often seen in technological miniature

components e.g. medical devices and organ-on-a-chip applications <mark>(Middleton *et al.*, 2018).</mark> The soft-tool discussed in this work was made using a material jetting AM system which provides significant throughput for prototyping of different cavity designs. Process characterisation has been carried out by the attachment of several sensing technologies on the soft-tooled μ-IM machine including thermal imaging and injection pressure monitoring. The in-line data has been collected for each single part/prototype made in back-to-back cycles carried out by an automated μ-IM machine. By doing this, a low - medium volume manufacturing scenario was mimicked and presented. State-of-the-art optical surface metrology was used for dimensional quality assessment of the parts and the deformation of the soft-tool due to processing. Multi-channelled process data collected for each part have been analysed in detail where cross-correlations between quality indicators are also presented for future reference and process development. The work emphasises that data-rich approaches should be implemented for soft-tooled product development because of challenging process environments including very small cavity features to replicate and soft-tool deformation. The aim and scope of this research can be summarised as following:

- To characterise the soft-tooled μ-IM process by using in-line process measurements,

- To quantify the changes on the soft-tools and prototypes that occur in an automated, soft-tooled μ-IM process,

- To present and link in-line collected process data with quality of the moulded parts,

- To contribute and comment on how data-rich approaches for soft-tooling can be utilised.

Methodology

Soft-tool design and additive manufacture

A soft-tool insert in a circular shape incorporating a disc-shaped double cavity design was made using a Stratasys J750 material jetting prototyping machine (Figure 1a). Build settings were configured using GrabCAD Print software (v 1.62.8.14676, Stratasys Ltd, USA). The build was made in 'high-quality' and 'glossy finish' settings with a 14 μm layer thickness in the z-axis. A white, translucent resin (Vero PureWhite - RGD837, Stratasys Ltd, USA) was used as the soft-tool material which provided sufficient rigidity and flexibility for processing and fixation of the insert to the bolster, respectively. Table I shows the physical properties of the cured resin used for printing the soft-tool. Details of the product design can be seen in Figure 1b, and a technical drawing is shown in Figure 1e. The soft-tool insert has an outer diameter of 55 mm with a thickness of 10.4 mm. A recess was machined in a 36 mm thick bolster cavity plate (K20/095x095x36/.1.1730, HASCO-In ternorm Ltd, UK) with the same dimensions as the insert (Figure 1c). 20 mm grooves were machined on the sides of the bolster cavity for easy removal of the insert. A single 3 mm ejector pin in the centre of the insert was sufficient for demoulding. The soft-tool insert was first loosely attached on the ejector pin using a plastic mallet and then was pressed in the recess using the clamping unit of the μ-IM machine. This removed any excess amount of material and sharp edges of the soft-tool by shaving off, providing a very tight fit after the pressing. The soft-tool, the housing bolster cavity plate and the ejection system were located on the moving-half of the mould (Figure 1c). The fixed-half consisted of a flat cavity plate with the same outer dimensions as the bolster (Figure 1d).

The double cavity design in the soft-tool with microfeatures allows characterisation of different aspects of the micromoulding process. One side of the disc-shaped double cavity was left blank for tests that could be of interest in the later stages such as deformation measurements, and the counterpart was designed to have micro-features for the assessment of the filling process. The

micro-features used in the present soft-tool design were 3 pairs of prismatic protrusion and recesses with a triangular profile, each having 600 μm depth or height, with a 700 μm base width (Figure 1e). The top angle was 60°C for the prismatic shape. Each pair of the microfeatures were placed progressively away from the gate with ~3.5 mm distance for the evaluation of micro-replication and possible deformation on the soft-tool. A single, circular recess with 600 μm depth and 800 μm diameter was also placed at the far end of the cavity where the replication would be most sensitive to the process variations and pressure drops during the filling process (Griffiths *et al.*, 2014; Gülçür and Whiteside, 2021; Gülçür *et al.*, 2021). The disc shaped main cavity had a diameter and thickness of 13 and 1.25 mm respectively. A considerably high draft angle of 10° was assigned on the sides of the part for making the part ejection as easy as possible. A relatively wide, fan-type gate, with a width and depth of 5 and 1 mm, was used. Such a large cross-sectional area allowed easy filling of the circular cavities, avoiding premature solidification of the flow front.
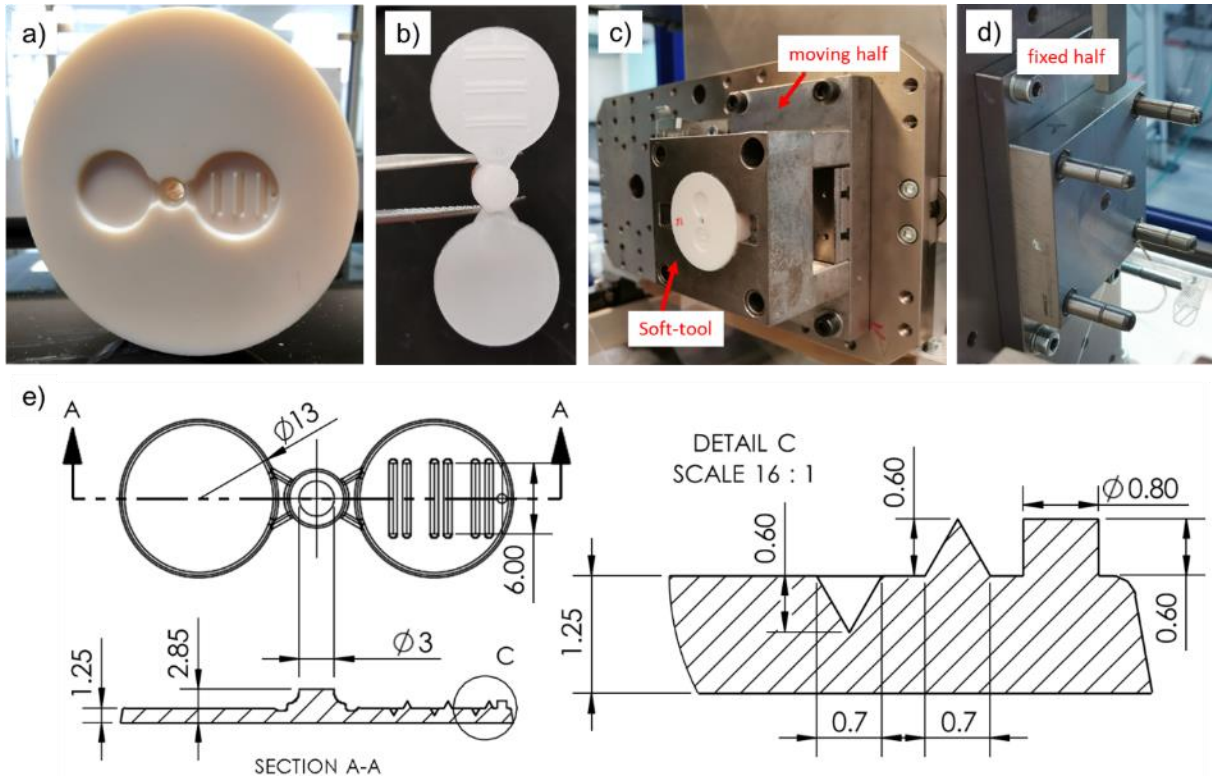
Figure 1 Details of the tool and product design: a) An image of the soft tool; b) an image showing the product/moulding; c) image showing the moving-half of the mould assembly; d) image showing the fixed-half of the mould assembly; e) the technical drawing showing the dimensions of the product design including the microfeatures.

Table I Physical properties of Vero PureWhite -RGD837 manufactured by Stratasys (Stratasys, 2022).

Properties	Value & units
Tensile strength	40 – 55 MPa
Modulus of elasticity	2200 – 3000 MPa
Heat deflection temperature (HDT)	45 - 50°C
Glass transition temperature (T_g)	52 – 54°C
Polymerised density	1.17 – 1.18 g/cm^3

The soft-tool protrudes from the bolster surface by about 400 µm so as to rely on the clamping unit to flatten it against the flat fixed-half (Figure 2). This avoids the variations that might be caused as a result of the AM process due to residual support material or sharp edges on the

soft-tool. Figure 2a shows how the soft-tool was constrained within the bolster. The insert was completely constrained except for the removal dents placed on the side, which were aligned perpendicular to the polymer melt flow direction to reduce stresses and not to compromise the constraints on the soft-tool. Figure 2b depicts a cross section of the bolster and the soft -tool, and directions of the constraints on the ==contact surface== with the fixed-half.
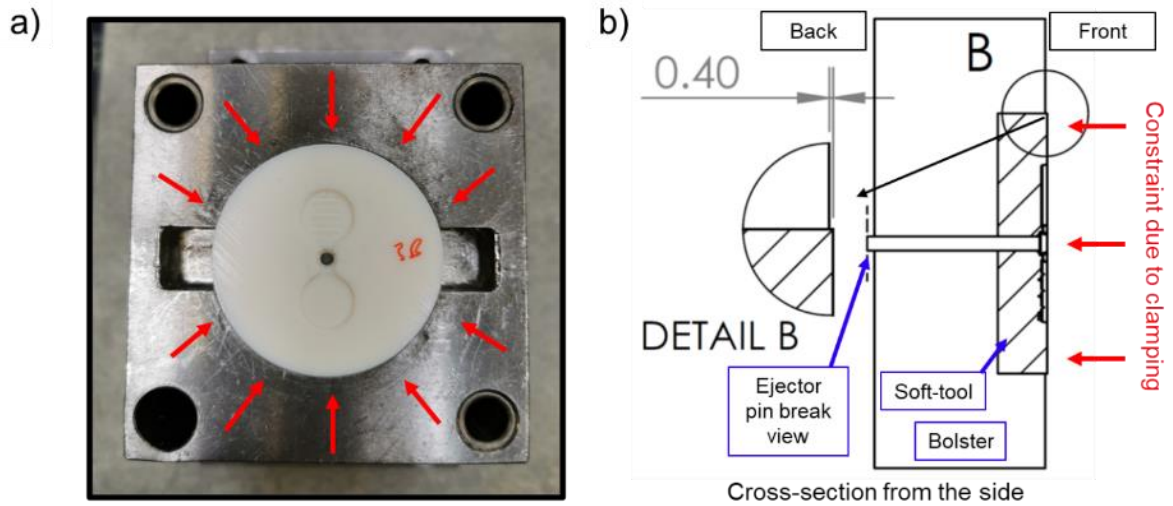
Figure 2 Constraints on the soft-tool: a) Image showing the soft-tool constraints within the bolster. The ejector pin can also be seen in the middle of the double cavity. Notice that the tool is completely constrained in the flow directions; b) Cross-section of the bolster and the soft-tool showing the constraints due to the clamping.

Soft-tooled micro-injection moulding

Manufacturing runs have been carried out on a Microsystem50 (Wittmann - Battenfeld UK, UK) µ-IM machine using a polypropylene (PP) resin (C711-70RNA, Braskem Europe, Germany). The machine is specifically designed for microsystem applications with 1.1 cm^3 theoretical maximum shot size with a dedicated dosing unit and a 5 mm injection piston. The filling process on the machine is controlled by monitoring the pressure value measured at the back of the injection piston for achieving superior switch-over (S/O) behaviour for replication of miniature cavities as small as 0.5 mm^3 (Whiteside *et al.*, 2005). Mould temperature control was not used in the experiment to keep the prototyping runs as simple as possible, allowing the natural thermal profile of the moulding trials to be determined. Table II summarises the processing settings used for the manufacturing runs. The machine was set to run in automatic mode and 100 parts were collected from back-to-back cycles with a cycle time of approximately 29 seconds. Minimum moulding parameters (injection pressure, melt temperature, clamping force) were used where possible for minimising the deformations on the insert that could occur due to shear heating or high pressures. The manufacturing cycles were set up in the manner that the parts were ejected automatically and collected through a chute located below the clamping unit. The soft-tool endured the whole manufacturing process and kept its outer dimensional integrity until the end without cracks or catastrophic mechanical failures and was still usable.

Table II Process parameters used in the soft-tooled manufacturing runs.

Melt temperature (°C)	Injection velocity (mm/s)	Switch-over (S/O) pressure (bar)	Packing or holding pressure (bar)	Packing duration (s)	Clamping force (kN)	Cycle time (s)	Shot size (cm^3)
190	200	150	200	6	45	29	0.445

In-line process monitoring

The thermal camera (Xi 410, Optris GmbH, Germany) used in the present work has a resolution of 384 x 240 pixels, a spectral range of 8-14 μm and a measuring accuracy of ±2°C. Figure 3a and b show thermal images of the mould surface before and after the ejection of the 50th part. The purpose of thermal imaging acquisitions was to monitor the surface temperature progression which may influence the filling process. This was achieved by recording three different temperature values from points of interest (POI). The first POI is the maximum temperature on the sprue (T_{sprue}) before the part is ejected. The second and third POIs are the maximum temperatures coming from the whole area of the soft-tool (T_{max}) and the maximum temperature measured on the micro-structured cavity (T_{max-c}). These values were recorded for each of the 100 parts.

Injection pressure data used by the machine control were recorded for each of the samples produced. An indirect force measuring pin (Type 9243B, Kistler Group, Switzerland) at the back of the 5 mm injection piston was used on the Microsystem 50 (Griffiths *et al.*, 2014). An electromagnetically shielded breakout cable connection was made to the Kistler 5039A amplifier at the μ-IM machine which feeds the pressure measurement output to the controller. Pressure data was collected through the analogue input channel of a myDAQ (National Instruments, USA) data acquisition device using a LabVIEW 2020 based data capturing interface (National Instruments, USA). The pressure readings were acquired at a rate of 1 kHz and calibrated using a two-point method according to the holding pressure value (200 bar) set at the machine control. A Savitzky-Golay filter was applied digitally using OriginPro 2021b (OriginLab Corporation, USA) analysis software to smooth and eliminate mechanical and electrical noise effects in the data for a better comparison of data sets for calculating pressure integrals. Figure 3c illustrates the injection pressure data from the first cycle. The faded, black curve shows the unfiltered, raw pressure acquisition data. As a quality or process indicator, the

mathematical integral of the pressure curve during filling and packing phases (A_p) was calculated for each sample from the filtered curves based on trapezoidal rule. The integration range used was from the value at which the pressure value turns positive until the end of packing.
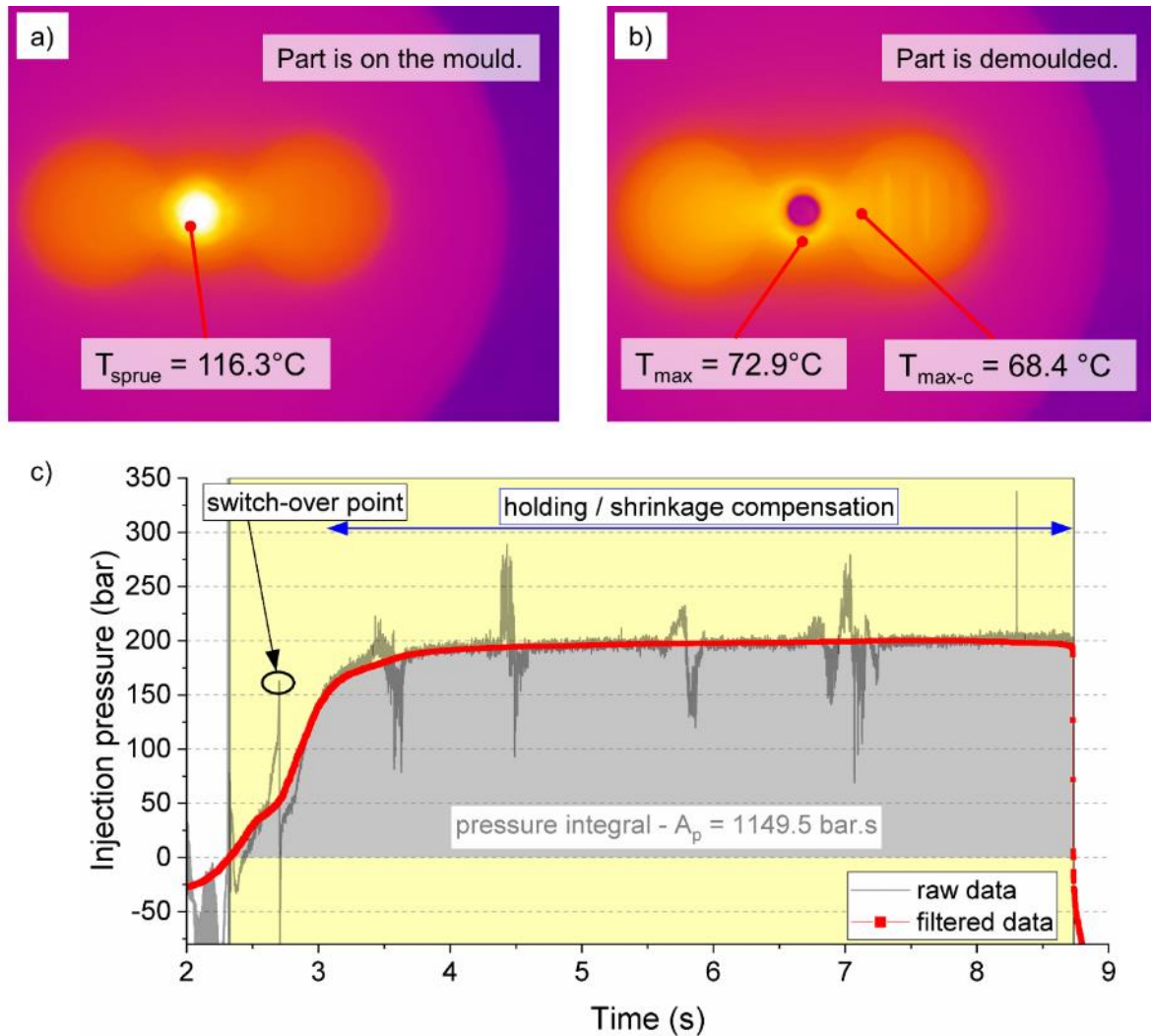

Figure 3 In-line process monitoring for soft-tooled μ-IM process: a) Thermal image showing the soft-tool insert before the ejection of the 50th part and location of T_{sprue}; b) a thermal image showing the soft-tool insert after the ejection of the 50th part and locations of T_{max} and T_{max-c}; c) injection pressure profile recorded from the first moulding cycle showing important phases of the filling and calculation of the pressure integral area, A_p. Thermal images are rotated 90° clockwise with respect to tool configuration given in Figure 1. Mechanical or electrical noise can be seen in the shaded raw pressure data.

Dimensional characterisation of parts and the soft-tool

Off-line or in-line dimensional product measurement methods such as focus variation microscopy, telecentric imaging and coherence scanning interferometry are widely used for quality assurance of miniature products (Romano *et al.*, 2019; Santoso *et al.*, 2022; Gülçür *et al.*, 2021; Whiteside *et al.*, 2005). In the present work, a laser-scanning confocal microscope (LEXT – OLS5000, Olympus UK & Ireland,) was used for dimensional characterisation of the soft-tool and the moulded parts. Measurements were carried out offline. Acquisitions on the soft-tool were made using a 5x objective lens without any filtering on the 3D data. Nine measurements were taken in manual mode with multiple baselines for decreasing the measurement bias.

For moulded prototypes, a 10x objective lens was used for making the acquisitions less susceptible to noise and reduction of measurement errors. Stitching setting were used on the microscope resulting in a 3D acquisition of the micro-features on a 7 x 10.5 mm area. 2D height profiles are often used in telecentric imaging and quality assurance of miniature products and the same approach also implemented in the present work (Gülçür *et al.*, 2021). For the simplification of the micro-replication assessment, 2D height profiles measured only from the circular feature located at the end of the cavity.

Figure 4 summarises the measurement strategy on the mouldings. A 2D and 3D image of the scan can be seen from Figure 4a. Laser scanning confocal microscope acquisitions were carried out on the first 10 and every tenth part until the last, 100th sample. For each replica, the protrusion height (h_p) was measured 3 times according to randomly chosen axes (Figure 4b). Height differences of the protrusions coming from different cycles can also be seen from Figure 4b. The 2D and 3D images provided in Figure 4a also signify the part-filling aspect of the moulding process and possible variations in micro-replication.
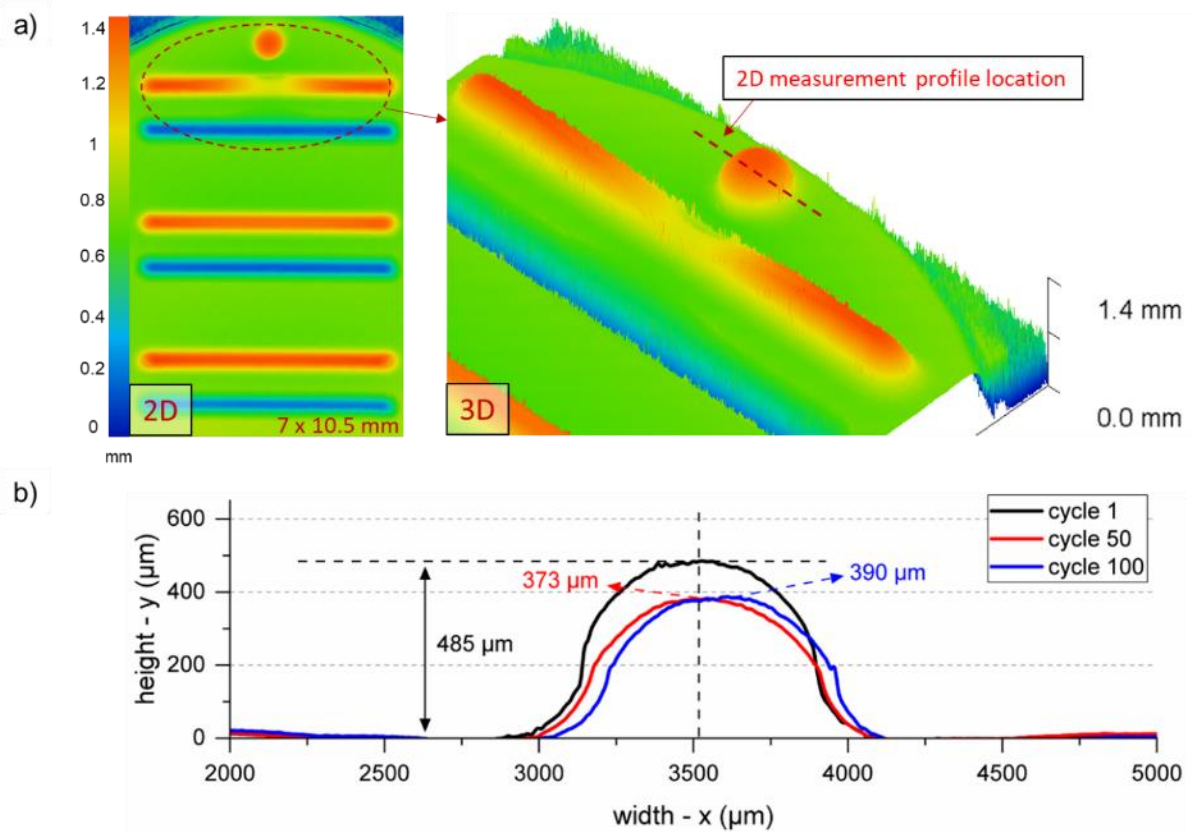
Figure 4 Product measurement strategy for the mouldings: a) 2D and 3D images showing the main features and the 2D profile measurement location; b) 2D profile data and measurement of h_p for cycle 1, 50 and 100.

Complementary measurements

A dynamical mechanical thermal analysis (DMTA) test was carried out for the validation of the T_g of the virgin soft-tool material. A DMA Tritec 2000 (Mettler – Toledo UK, UK) thermo-mechanical analyser was used in the single cantilever mode. The details and parameters of the measurement are given in supplementary data.

Results & discussion

Dimensional characterisation of microfeatures on the soft-tool

Table III shows the nominal and actual dimensions of the microfeatures on the soft-tool ==used==. It can be seen from the data that the material jetting prototyping machine is able to produce proud features closer to nominal dimensions with a decent repeatability compared to the recesses. As expected, the error or the deviation in the recess measurements is more pronounced. The reason for this is that during the jetting of each layer at the printer head, the uncured resin tends to spread and hence result in less accurate prints for recesses. The same behaviour is not particularly dominant for the circular feature at the end of the cavity. This is due to the fact that the circular cut is slightly wider (800 μm) and hence the resin spreading or rounding effect becomes less pronounced.

Table III Nominal and actual dimensions of the micro-features on the soft-tool and associated variations. The errors are provided in standard deviation form.

Feature / measurement	Triangular protrusion height measurements	Triangular recess depth measurements	Circular feature depth measurement
Nominal (μm)	600	600	600
Measured (μm)	566.1 ± 11.6	482.3 ± 25.8	588.8 ± 6.3
Coefficient of variation (%)	2.04	5.35	1.07

Temperature and injection pressure progression

Three characteristic soft-tool surface temperature values were extracted for each 100 cycles using PIX Connect software (version 3.16.3092.0, Optris GmbH, Germany) and plotted against cycle numbers in Figure 5. Temperature indicators have significant differences in their values due to their acquisition location. High variance in T_{sprue} can be attributed to the height and flashing variations on the sprue of the part. This is the closest section of the micromoulding cavity to the nozzle heater of the injection unit where its temperature is being controlled with a PID (proportional integral derivative) unit, that could cause fluctuations in the melt temperature near it. The other two (T_{max} and T_{maz-c}) measurements less variability in the data over the cycles. It can be seen that T_{max} and T_{max-c} mostly stabilise after the 10th cycle at 80 and 75°C, respectively. Between 11-100 cycles the temperature increase is seen continuously until the last moulding, however at a lower rate. The rate of increase in temperatures were also quantified by calculating the slope (gradient) for the data as can be seen from Figure 5. The inability of the polymer to conduct the heat to its surroundings keep it within the cavity, with a marginal increase in temperature every cycle. The fluctuations occurring after the 30th cycle are once again likely to be caused by the PID temperature control near the nozzle of the injection unit and shear heating. Overall, it is expected that temperature readings taken from the soft-tool surface rather than the sprue are more likely to represent the overall characteristics of a process or product indicator. This is due to T_{sprue} being affected by the sprue height variations and showed a much greater level of scatter, especially after the 10th cycle (Figure 5).
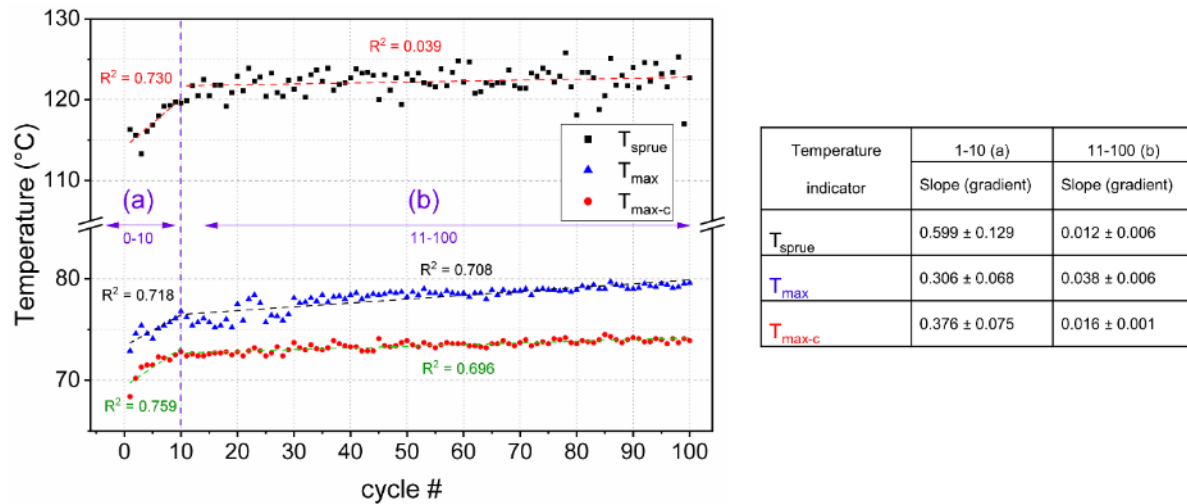
Figure 5 Temperature progression in the soft-tooled µ-IM process and associated slope values for cycles 1-10 and 11-100.

Differences in injection pressure profiles have been found from the 1st until 100th cycle, although the process conditions were kept the same through the runs. The data given in Figure 6a depict that the pressure sustained in the cavity is decreased according to the visible deviations in the curves. These pressure drops have been quantified by the data given in Figure 6b, which depicts the decreasing progression of A_p, the pressure integral. The correlation for this decrease is low and inconsistencies are present, due to the filtering of the injection pressure curves and the integration boundaries which is dependent on the judgment of the user. Continuously increasing mould surface temperatures presented in Figure 5 and a decrease in the pressure integrals are completely the opposite to what would have been experienced in industry standard steel moulds (Whiteside et al., 2005). Conventional behaviour for metal tools is that increased mould temperatures help the polymer to maintain its low viscosity and hence help sustain the cavity pressure for longer periods. However, the soft-tool was expected to be prone to deformations and its relevance to pressure changes had to be analysed.

Since there was not an in-line capability for capturing the whole 3D surface of the soft-tool after each moulding cycle which lasts ~29 s, the deformations occurring on the soft-tool had to

be measured using an indirect approach. This entails the analysis of 3D measurements acquired on the mouldings and quantification of deviations. A flat line has been drawn on the 3D data towards the bottom of the acquisition, which is the nearest to the gate and profiles have been extracted for the 1st and every 10th moulding until 100th (Figure 6c). This data shows if the flat profile and dimensional integrity of the tool is changing over the course of the manufacturing process. Figure 6c depicts the profiles extracted from the pristine surface, 50th and 100th moulding and the location of the acquisition. The data was calculated as a "cross-sectional area difference" which were termed as A_{dev} – areal deviation near the gate. Data given in Figure 6d shows that the deviation progressed linearly throughout the cycles. This result suggests that there could be a significant deformation in the soft-tool over the cycles which effects the dynamics of the process (filling, packing etc.), where the sustained pressures decrease even though the surface temperature increases. Further clarification was needed to be sure that decreasing pressure integrals were caused by soft-tool deformation and hence the gate profiles before and after the processing were analysed.
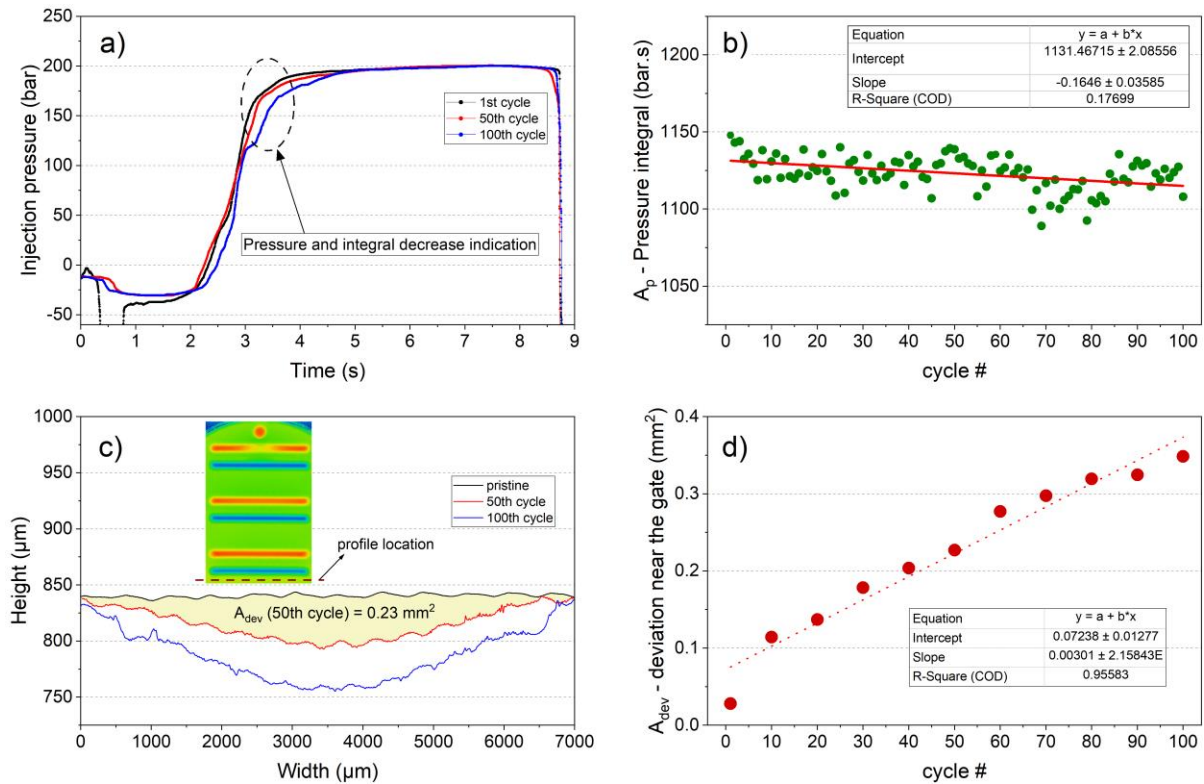
Figure 6 Pressure data recorded from soft-tooled μ-IM cycles: a) Injection pressure profiles showing differences between the 1st, 50th and 100th cycles; b) pressure integral progression from the 1st to 100th cycles.

The gate section is an important design consideration, particularly in μ-IM where improperly designed or deformed gates can cause short shots easily (Marhöfer *et al.*, 2016). Due to the aforementioned limitation in 3D data acquisition cycle by cycle, gate profiles have been extracted only from the pristine state of the soft-tool and after 100 cycles for comparison (Figure 7a). Profiles given in the figure show that the gate section of the soft-tool significantly deformed by approximately 200 μm in height and 150 μm in width resulting in an approximately 28% reduction in cross sectional area. The deformation near the gate is expected and very understandable, as the hot nozzle of the injection unit also stands flush with the soft-tool during the moulding process, hence making it easy for losing its dimensional integrity. This behaviour was evidenced by the imprint of the nozzle shown in Figure 7a and its imprint

has left a significant deformation on the soft-tool as can be seen from the profile. The correlation plot shown in Figure 7b depicts the relationship between the A_{dev} and A_p with a negative trend, which supports the behaviours shown in Figure 6, where deformations in the tool were correlates with the pressure integral about 50% accuracy. Although the analysis in Figure 7 is based on the initial and final state of the soft-tool, it is in correspondence with the progressive deformation occurring in the soft-tool and making it necessary to study the replication efficiency of the mouldings and the overall volume reduction in the soft-tool.
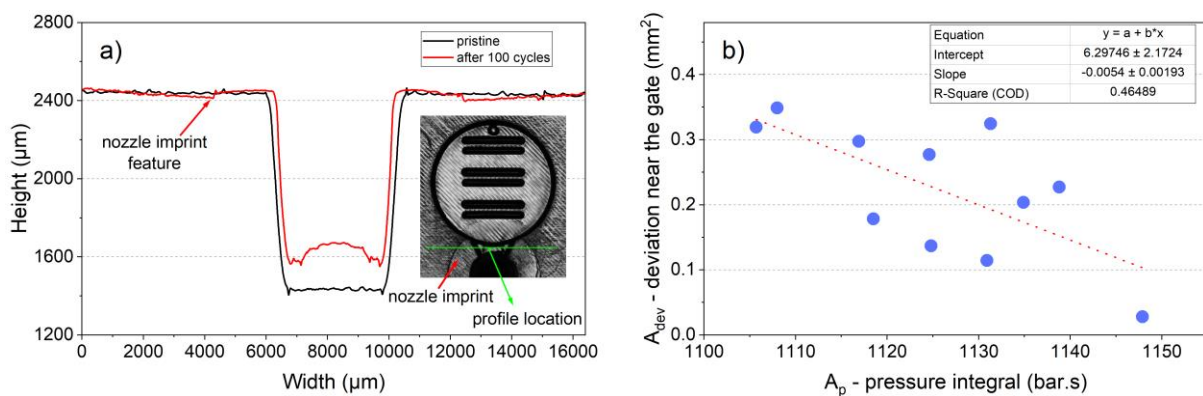

Figure 7 Gate profiles of the soft-tool: a) Comparison of the profiles of the gate on the soft-tool in pristine state and after 100 cycles; b) scatter plot showing the relationship between A_{dev} and pressure integral.

Micro-replication progression

Figure 8 shows the progression of h_p, which is the indicator of the micro replication quality vs cycles before and after processing. Data in Figure 8a show that the circular protrusion at the end of the cavity is replicated with approximately 85% efficiency in the 1st cycle with 498 ± 23 μm height. h_p then deteriorates steadily until the 40th cycle, then stabilises approximately at 400 μm. Once again, this is an unexpected behaviour as the mould surface temperature increases steadily (see Figure 5) and it would keep the viscosity of polymer melt relatively low, which helps replicating micro and nano features in the mould cavities in the conventional sense.

However, worsening micro-replication over the cycles is also in agreement with the pressure integral and deformation data given in Figure 6. On the other hand, the injection pressure data is acquired indirectly from the back of the injection piston, and it is plausible that it might provide limited information regarding h_p. The protrusion features on the soft-tool were also inspected on the pristine and on the insert used for 100 cycles, to quantify if any particular deformation occurred in terms of depth. The profile data in Figure 8b for the protrusion feature on the soft-tool does not show changes that could result in a deterioration on the h_p. In the light of these findings, the reasons for the decrease in microreplication efficiency can be postulated as following:

- The cavity expands due to the increasing soft-tool temperature, and the fixed shot size does not compensate for this volume expansion, hence resulting in short shots and worse micro-replication. However, this is unlikely as severe deformation is detected near the gate and a significant volumetric decrease is expected in the micromoulding cavity.

- Critical sections of the soft-tool (e.g. gate – sprue region) become deformed and reduction in cavity size leads to a filling process that would need more pressure for a successful filling event in terms of micro-replication. This might also increase the pressure overshoot at the S/O point (move from velocity to pressure controlled filling during moulding).
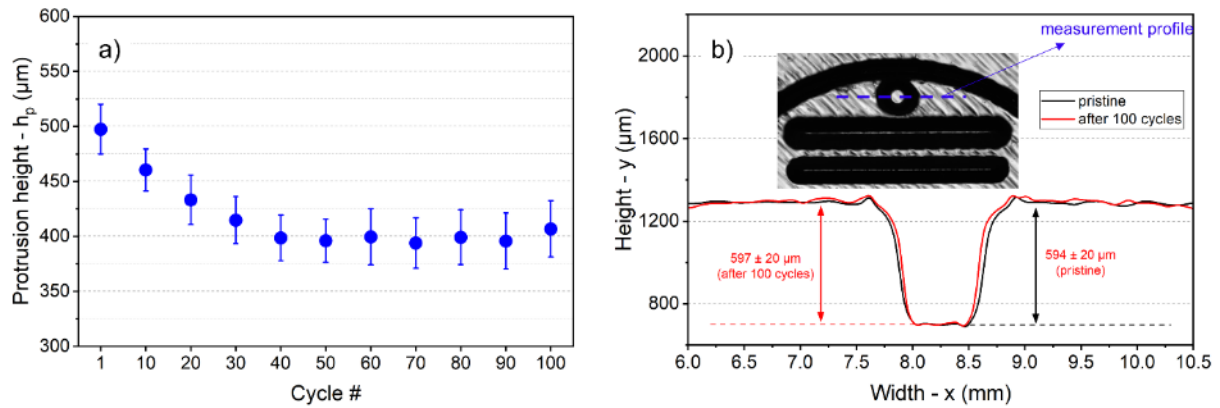
Figure 8 Micro-replication data from the process: a) Data depicting protrusion height (h_p) or micro-feature replication vs cycles, b) Comparison of the profiles of the protrusion feature on the soft-tool in pristine state and after 100 cycles.

Both statements given above are plausible given the fact that soft-tools are known to expand or deform more severely than conventional mould tools due to being made out of polymer. For investigating if the S/O point is affected by the deformation occurred in the cavity size, analysis of the unfiltered pressure data near the pressure-controlled S/O points was performed. The S/O point is of great importance for filling control in micromoulding, because of the extreme injection speeds, flow rates and associated momentum of the injection piston and the unit (Whiteside *et al.*, 2005; Gülçür and Whiteside, 2021). Due to significant gate cross section decrease at 28%, an overshoot in injection pressure can be expected. The μ-IM machine used in this work has a very responsive pressure-controlled S/O behaviour where the changes in the volume of the cavity could be detected or compensated [33]. The S/O point is defined as the pressure value at which the machine changes its velocity controlled behaviour to pressure control, by continuously monitoring the injection pressure value and switching-over to pressure control at a pre-defined value. This resulted in a pressure increase up to 150 bar in the current study, and then a sudden decrease due to machine control followed by an increase up to 200

bar and packing for 6 seconds. Due to the momentum of the injection unit and high injection velocities, the pressure value usually exceeds the S/O value, and the system usually switches-over at a value with an overshoot.

The graph given in Figure 9a shows the injection pressure profile for the 1st cycle and depicts the filling behaviour using the unfiltered injection pressure signal. The S/O point at 163.1 bar was detected in the 1st cycle and the sub-graph show details regarding the machine response which occurred over a very short period of 4 ms. The S/O peak values were extracted for all 100 samples in the same manner (Figure 9b). The data in Figure 9b show that S/O characteristics were not changed due to the dimensional changes that might have occurred in the micromoulding cavity. However, the peak values were expected to have an inherent inconsistency due to the mass and associated momentum during deceleration of the injection unit (Whiteside *et al.*, 2005). Hence, increasing the data acquisition rate for this pressure measurement, and investigation of pressure integrals near the S/O point could provide better insights regarding the changes in the soft-tool cavity and filling. Another explanation for the scattered behaviour of S/O values can be made as following. Increasing surface temperatures which would help better replication and decreasing gate size which could cause short-shots work against each other simultaneously and make the assessment difficult. In the light of this analysis, dimensional characterisation for pristine and processed soft-tool cavities was carried out for the validation of changes that might be occurring to further explain the aforementioned replication behaviour.
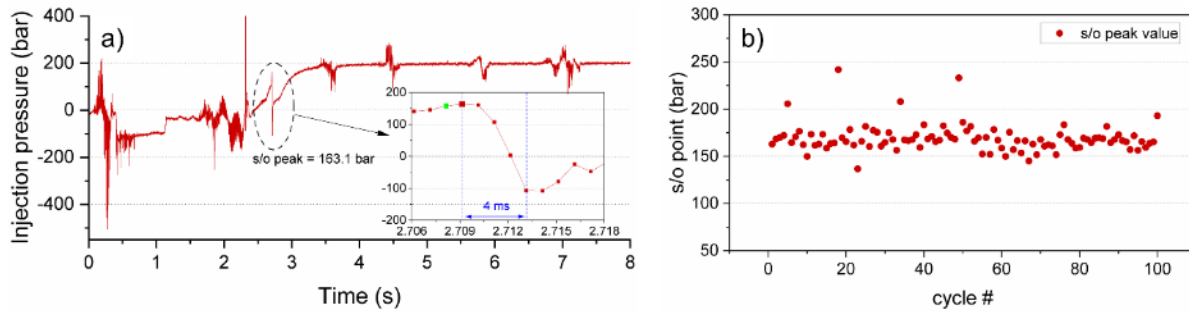
Figure 9 S/O characteristics in the soft-tooled µ-IM process: a) unfiltered pressure data taken from the 1st cycle and depiction of S/O point; b) S/O peak values vs cycles.

Soft-tool characterisation before and after processing

A comparison was made between the 2D measurement data given in Table III and the data acquired from the used soft-tool after 100 cycles. Figure 10a shows the changes on the soft-tool, including deformation near the gate, and an imprint of the nozzle in the centre due to its high temperature. The periodic lines with 45° alignment are due to the material jetting process. 2D profiles have been extracted from the blue and green dashed lines which correspond to locations near the gate and in the middle of the flat side of the cavity. The deformation near the gate seems to be quite prominent where approximately 300 µm deviation was present from the reference as shown in Figure 10b. Deformation on the flat side of the cavity was also detected as can be seen from Figure 10c. The reasons and nature of these deformations can be attributed to:

- Since the soft-tool is almost completely constrained on all sides, the expansion occurs towards the only non-constrained section of the soft-tool, which is the micromoulding cavity itself,

- The hottest areas are expected to be on the micromoulding cavity, rather than the surroundings which will make the cavity even more susceptible to deformation.

- The resistance to the ejection due to the adhesion forces between the parts and the soft-tool contribute to cavity deformation in the ejection direction at higher temperatures.
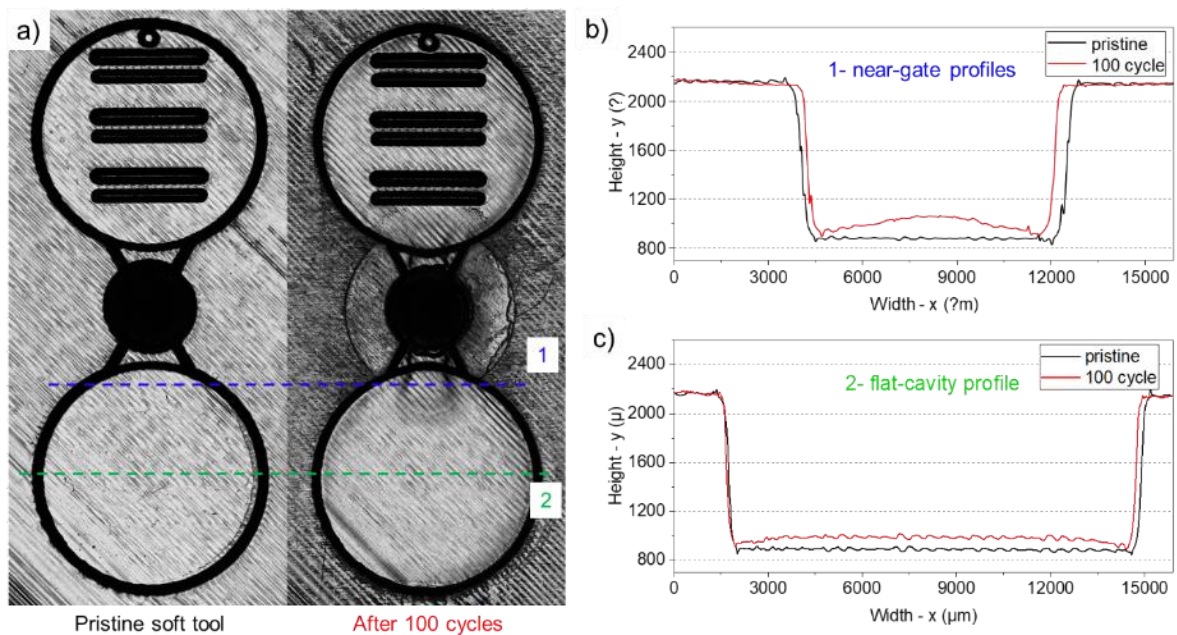

Figure 10 Comparison of pristine and processed soft-tool cavity: a) optical images taken from the laser scanning confocal microscope showing the pristine and cavity after 100 cycles with profiles of interest (shown in blue (1) and green (2) dashed-lines); b) near-gate profile comparison for pristine and processed insert; c) flat-circular cavity profile comparison.

Volume calculation for the flat and the micro-structured sides of the soft-tool was carried out using OLS4100 software (version 3.1.15, Olympus UK & Ireland, UK) for quantifying the overall dimensional changes in the micromoulding cavity. Volumes were calculated by using reference planes on the top surface of the soft-tool with corresponding regions of interest on the circular cavities. Each calculation was made 3 times. The results in Table IV show that the volume for the flat and the cavity with microfeatures decreased 8.2 ± 0.7% and 13.2 ± 0.7% respectively. More severe volume reduction in the cavity with microfeatures can be explained by its larger surface area than the flat cavity resulting in more expansion in the unconstrained direction at elevated temperatures.

Table IV Total volume calculation of the circular soft-tool cavities. Errors are given in standard deviation.

Pristine		After 100 cycles	
Flat cavity	Cavity with μ-features	Flat cavity	Cavity with μ-features
172 ± 1 mm^3	177 ± 1 mm^3	158 ± 1 mm^3	154 ± 1 mm^3

2D and 3D temperature mapping data of the mould insert after the 50th cycle is given in Figure 11a and b. Earlier cycles showed similar temperature distributions and contours, but with lower temperature values. The data supports the findings in Figure 5 by having the highest temperature distributions near the sprue and gate regions. The contour of the temperature near the gate is also similar to the deformation occurring in the same region as was presented in Figure 7 and 10. Another significant feature of this representation of the data is the notable difference between the cavity temperatures and the insert material surrounding it. The soft-tool temperature around the cavity can be assumed approximately 40°C according to the scales. This difference is obviously due to the low thermal conductivity of the insert material, and this also contributes to the deformation of the cavity in the same direction with the ejection/demoulding where the hottest regions are located.

The T_g (52 - 54°C) of the soft-tool material was confirmed with a single-cantilever DMTA analysis on the pristine Vero PureWhite by analysing the storage modulus (G'), loss modulus (G") and tanδ parameters (see Appendix for details). Figure 11c shows the DMTA data for the soft-tool material. According to the G' and G" curves, the mechanical degradation starts around 50°C, and the T_g was determined to be 56°C according to the onset of the G' and peak value of the G" which confirms the value in the datasheet (*Measurement of Glass Transition Temperatures by Dynamic Mechanical Analysis and Rheology*, 2022). The material shows a

significant mechanical property degradation between 60-80°C. Because of this feature, one might expect severe deformation on the soft-tool compared to the one presented in this work; however, it should be noted that this is a UV and heat curable resin, and the soft-tool material is expected to stiffer as it is being cycled during the process. Therefore, although the DMTA analysis confirms the soft-tools initial thermomechanical properties, the thermal cycling history of the used soft-tool is much more complex. By heat treatment or post-processing through UV curing, the soft-tool can become mechanically more robust and 13% cavity deformation we presented in Table IV can be reduced and prevented. As a result, although limitations regarding the feature size are present, the soft-tools' lifespan can significantly be improved.
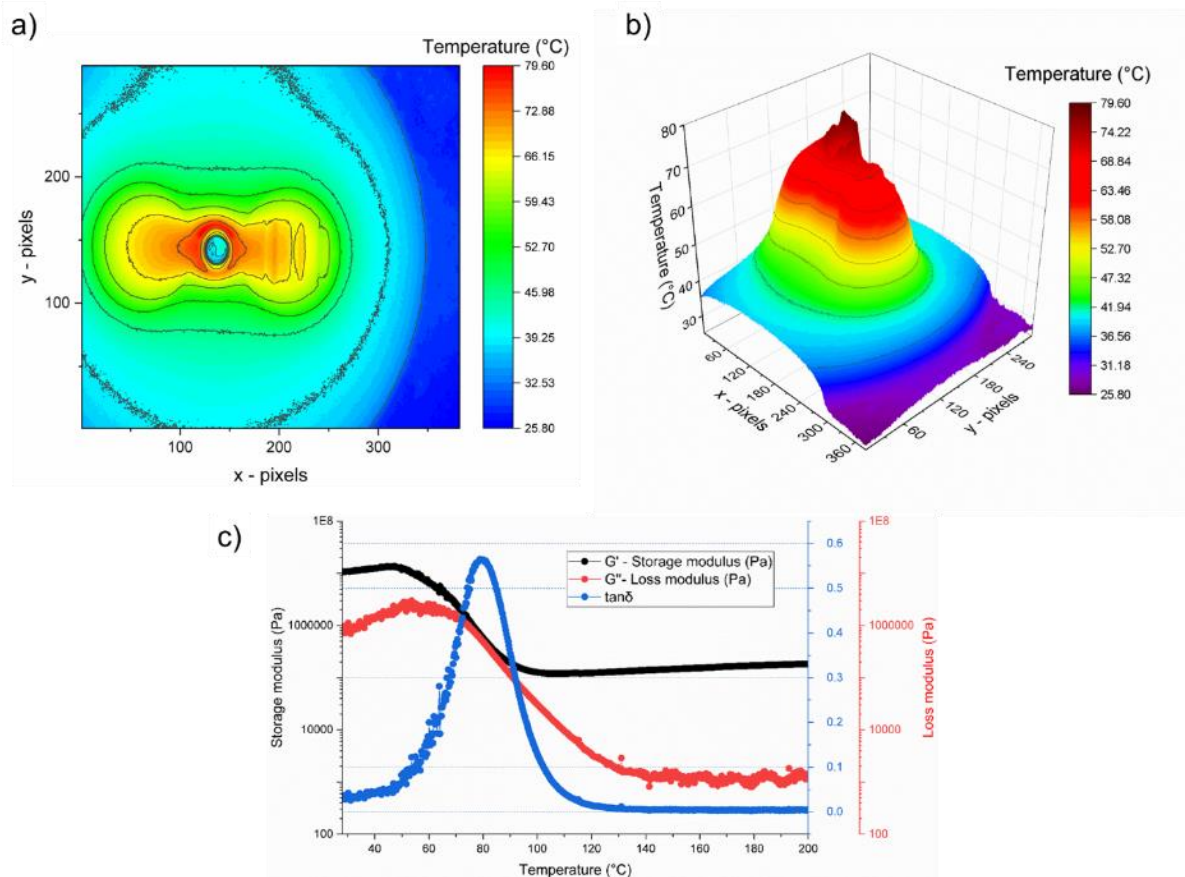

Figure 11 Temperature mapping data taken from the 50th cycle: a) 2D temperature mapping; b) 3D temperature mapping; c) DMTA data showing G', G'' and tanδ parameters for the soft-tool material.

Filling and quality prediction in soft-tools using process data

Correlations between cavity filling (protrusion height – h_p), temperature and pressure data were also studied for quantification of the data-rich aspect of the process. Scatter plots in Figure 12 show and quantify the linear relationships between micro-feature replication and process data. 19 data points were used, including the data taken from the cycles 1-10, in addition to the previous dataset for increasing statistical significance. Temperature data shown in Figure 12a taken from the sprue area (T_{sprue}) shows a moderate but inferior correlation as compared with the data given in Figure 12b and c for T_{max-c} and T_{max}. This is due to the variability in the measurement and imaging focus which was discussed also for Figure 5. T_{max-c} and T_{max} resulted in R^2 values of 0.731 and 0.906, respectively. The latter is a significant correlation since the filling in the soft-tool can be predicted at about 90% accuracy by only monitoring the process data coming from the thermal imaging, without additional off-line surface measurement methods. The difference between the correlations is marginal, which signifies that a more capable sensor could be beneficial for differentiation of temperature indicators.

Pressure integral (A_p) data given in Figure 12d exhibited a scattered behaviour, showing only a very slight positive trend ($R^2 = 0.262$) between the in-line collected data and h_p which is not statistically significant. Various reasons contribute to the inferior quality of the data here, such as the filtering/smoothing operation performed on the time-dependant pressure data for eliminating mechanical and possible electrical noise. More accurate measurements can be achieved through implementation of cavity pressure sensors or strain gauges on the mould or the μ-IM machine (Krizsma *et al.*, 2021; Gülçür *et al.*, 2020). Nevertheless, in-line capture of injection pressure has been extremely useful to detect the decreasing pressure trends in the soft-tooled rapid prototyping process for this work.

Data in Figure 12a and c also represent a sigmoid-like behaviour and 2 different states are visible. This is an indication that the replication and filling might be affected by a critical

temperature. Hence, logistic regression was performed to characterise process measurements'

capability to make a classification of parts or prototypes with acceptable quality.
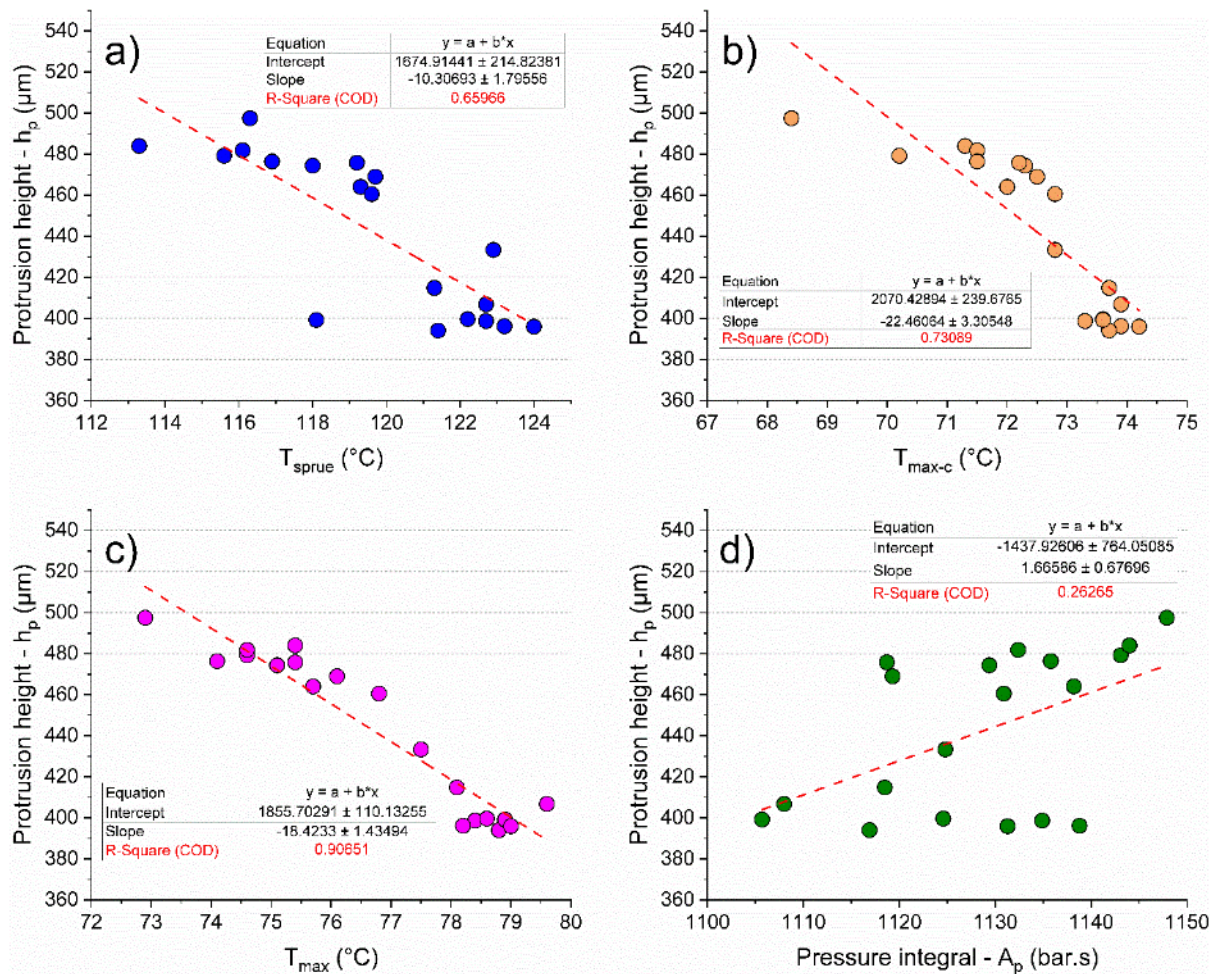
Figure 12 Scatter plots depicting correlations between process data and micro-replication: a) h_p vs T_{sprue}; b) h_p vs T_{max-c}; c) h_p vs ΔT_{max}; d) h_p vs A_p.

Scatter plots given in Figure 13 depict the deviations from the initial micro-feature replication

(Δh_p) as a function of temperature deviation (ΔT) which are calculated in the same manner.

These were simply determined by subtracting the values of the first cycle from progressing

cycles for h_p and all temperature values (see Appendix). The data in Figure 13 a,b and c show

a consistent trend indicating two states, which can be separated by a vertical critical

temperature value. The dimensional variations appear relatively stable below (and above) an

obvious critical temperature (T_c) as emphasised by a sigmoid curve (purple curve) fitted to the

Sigmoid fits were calculated using the logistic fit option in a data analysis software (OriginPro 2021b, OriginLab Corporation, USA) (*Help Online - Origin Help - 30.1.104 Logistic*, 2022). Parameters of the fitted functions are provided in the supplementary data.
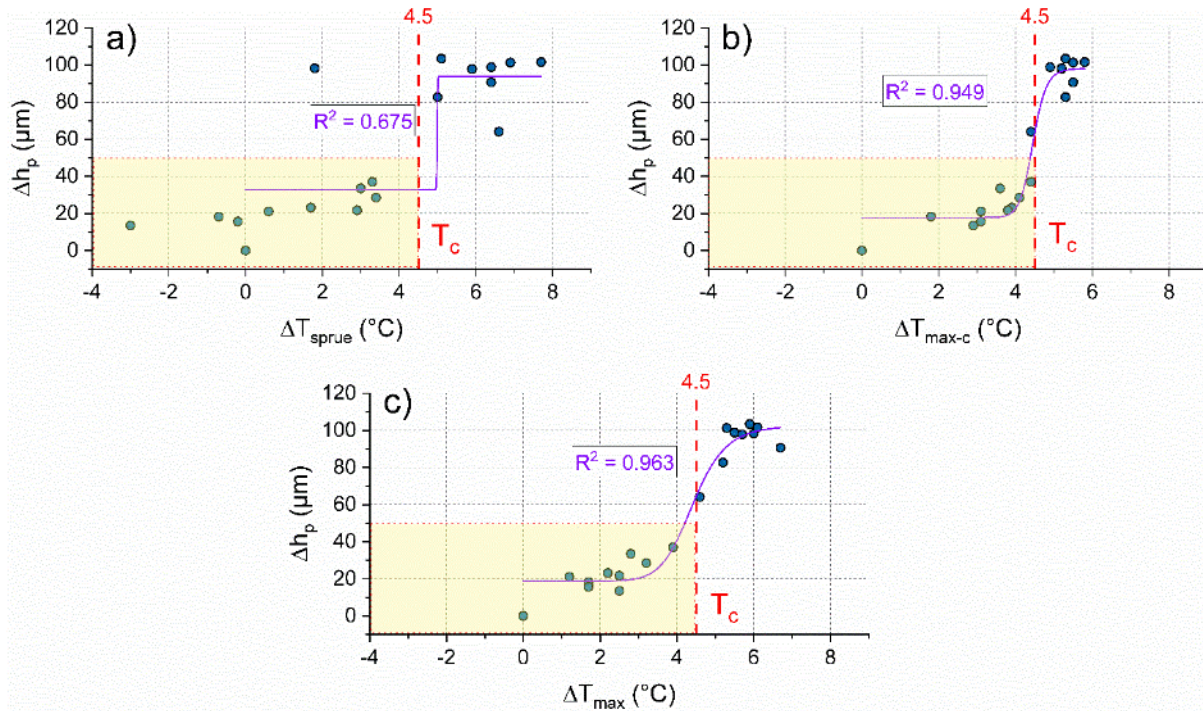
Figure 13 Scatter plots depicting the sigmoidal relationships between variation in micro-feature replication and variations in temperature: a) Δh_p vs ΔT_{sprue}; b) Δh_p vs ΔT_{max-c}; c) Δh_p vs ΔT_{max}.

Based on this sigmoid-like behaviour, the possibility of using in-line measurement data as a classifier of the moulding quality was evaluated. Logistic regression was performed with dichotomous states for the variables defined as below:

- For micro-feature replication (h_p), a deviation of 10% (~50 μm) was tolerated from the initial dimension (1st moulding). Above this cut-off value (indicated with T_c and shaded areas in Figure 13), the parts were considered outside tolerance.

- The cut-off point for the critical temperature variation is defined here as 4.5°C above the initial value based on the observations.

On this basis, we calculated the sensitivity and specificity for our classifier, using each 30% of the data from quality indicators as training set. For both T_{sprue} and T_{c-max}, we obtained a sensitivity of 100% and specificity of 75% (see Supplementary data for dichotomous classification tables), while T_{max} provided a perfect classification of 100% sensitivity and %100 specificity. To confirm this result, the receiver operating characteristic (ROC) was generated that yielded an area under the curve of 0.875 for T_{sprue} and T_{c-max}, and 1 for T_{max}. The robustness of the classifier is excellent, since adding a 10% tolerance to T_c (up to ~5°C) only reduces the sensitivity and specificity of T_{max} to 100% and 75%, respectively. Therefore, the results show that inline measurements enable us to carry out filling prediction and quality assessment based on their states, without the need for off-line measurements thereby greatly simplifying the quality control of the prototypes.

A global comment can be made that in-line collected process data shows excellent potential in quality prediction of the moulded prototypes and characterising the general behaviour of the soft-tooled μ-IM process. The quality of the collected data and insights that could be extracted from it can be improved using suggestions below:

- Implementing more capable sensors with higher measurement resolutions and sensitivities to extract data that are more representative of the prototype or filling quality,

- Usage of different type of sensor technologies (strain gauges, humidity sensors etc.) in addition to the present capability,

- Full automation of the data-post processing, where the data trends and implications will be presented real-time during the prototyping runs, allowing user to interfere or modify the process.

Conclusions

This work presented a detailed characterisation of a soft-tooled μ-IM process by using in-line collected data and surface metrology. A soft-tool design incorporating product with micro-features was used in an automated μ-IM machine for prototyping runs. Process and product quality indicators were defined and extracted from the in-line and off-line methods. Soft-tool cavity temperature, injection pressure and micro-replication progression were studied in a process mimicking a low or medium volume manufacturing setting. The key observations were:

- Permanent deformation was detected in the soft-tool micromoulding cavity and this was also in agreement with the temperature mappings acquired from thermal imaging. Although the cavity was permanently deformed, the soft-tool kept its dimensional integrity for over 100 cycles and showed local deformations near the gate, sprue, and circular cavity regions. Approximately 10% of reduction in the micromoulding cavity volume was found in the constrained soft-tool after 100 cycles. This is thought to result from continuous ejection/demoulding forces between the parts and the soft-tool cavity surface which is near its T_g.

- S/O characteristics of the process were also investigated with no implications associated with the deformation of the soft-tool.

- Correlations between the process and dimensional product data were analysed which allowed prediction of the filling level with about 90% accuracy.

- The most relevant temperature values to the filling were found to be from the surface of the soft-tool just after the ejection of the part.

Overall, the work provides a datum highlighting the significance of data-rich characterisation of soft-tooled prototyping and the importance of in-line sensor integration and monitoring. Novelties and significant outcomes generated through this work can be summarised as follows:

- An automated, soft-tooled μ-IM process for a sub-gram prototype was presented with no catastrophic tool failure.

- Multi-channelled data have been utilised for characterisation of the soft-tooled process.

- In-line monitoring provided a method to evaluate the quality of moulded parts.

- Suggestions have been made to improve the work present where more capable sensor technologies and dimensional characterisation should be used.

APPENDIX

Dynamical mechanical thermal analysis (DMTA) details:

DMTA sample was printed using Stratasys J750 material jetting prototyping machine using the soft-tool material (Vero PureWhite – RGD837, Stratasys Ltd, USA) with 4 x 40 x 10 mm dimensions. Single cantilever measurement was used for obtaining storage modulus (G'), loss modulus (G'') and tanδ parameters. The cantilever stood at a 7.5 mm distance from where the sample was fixed. Strain was applied on the sample at a 1 Hz frequency with a 0.02 mm displacement. The test was carried out from room temperature (25°C) to 200°C. Figure A below shows the measurement data.

Sigmoidal curve fit data

Data given below tables are the parameters of the sigmoidal fits applied to the data in Fig.11 of the manuscript.

Data for ΔT_{sprue}

Model	Logistic
Equation	y = A2 + (A1-A2)/(1 + (x/x0)^p)
Plot	devhp
A1	32.89838 ± 8.47237
A2	93.96965 ± 9.78305
x0	4.98954 ± 1749.14771
p	709.14527 ± 1.18678E8
Reduced Chi-Sqr	574.2481
R-Square (COD)	0.67557
Adj. R-Square	0.59447

Data for ΔT_{max-c}

Model	Logistic
Equation	y = A2 + (A1-A2)/(1 + (x/x0)^p)
Plot	devhp
A1	17.80289 ± 3.63655
A2	98.11551 ± 4.35687
x0	4.44954 ± 0.07063
p	25.54993 ± 12.23398
Reduced Chi-Sqr	90.37428
R-Square (COD)	0.94945
Adj. R-Square	0.93933

Data for ΔT_{max}

Model	Logistic
Equation	y = A2 + (A1-A2)/(1 + (x/x0)^p)
Plot	devhp
A1	18.87592 ± 2.88283
A2	102.6826 ± 6.24493
x0	4.4251 ± 0.16088
p	10.2937 ± 3.28159
Reduced Chi-Sqr	66.51621
R-Square (COD)	0.96279
Adj. R-Square	0.95535

Logistic regression data

Table below shows the raw data and dichotomous classification for the logistic regression analysis carried out.

cycle #	T sprue			Tc-max			Tmax			Ap - integral	hp		
	°C			°C			°C			°C	micron		
1	116.3	0	1	68.4	0	1	72.9	0	1	1147.9	497.4709	0	1
2	115.6	-0.7	1	70.2	1.8	1	74.6	1.7	1	1143.1	479.194	18.27685	1
3	113.3	-3	1	71.3	2.9	1	75.4	2.5	1	1144	483.9811	13.48977	1
4	116.1	-0.2	1	71.5	3.1	1	74.6	1.7	1	1132.4	481.826	15.6449	1
5	116.9	0.6	1	71.5	3.1	1	74.1	1.2	1	1135.8	476.36	21.11089	1
6	118	1.7	1	72.3	3.9	1	75.1	2.2	1	1129.4	474.3313	23.13962	1
7	119.2	2.9	1	72.2	3.8	1	75.4	2.5	1	1118.7	475.772	21.69892	1
8	119.3	3	1	72	3.6	1	75.7	2.8	1	1138.2	463.9934	33.47752	1
9	119.7	3.4	1	72.5	4.1	1	76.1	3.2	1	1119.3	468.9418	28.52904	1
10	119.6	3.3	1	72.8	4.4	1	76.8	3.9	1	1130.9	460.4959	36.97499	1
20	122.9	6.6	0	72.8	4.4	1	77.5	4.6	0	1124.8	433.3388	64.13205	0
30	121.3	5	0	73.7	5.3	0	78.1	5.2	0	1118.5	414.7749	82.696	0
40	122.7	6.4	0	73.3	4.9	0	78.4	5.5	0	1134.9	398.6575	98.81339	0
50	123.2	6.9	0	73.9	5.5	0	78.2	5.3	0	1138.8	396.143	101.3279	0
60	122.2	5.9	0	73.6	5.2	0	78.6	5.7	0	1124.6	399.6272	97.84372	0
70	121.4	5.1	0	73.7	5.3	0	78.8	5.9	0	1116.9	394.0285	103.4424	0
80	118.1	1.8	0	73.6	5.2	0	78.9	6	0	1105.7	399.2148	98.25608	0
90	124	7.7	0	74.2	5.8	0	79	6.1	0	1131.3	395.8993	101.5716	0
100	122.7	6.4	0	73.9	5.5	0	79.6	6.7	0	1108	406.8142	90.65668	0
		sensitivity	specificity		sensitivity	specificity		sensitivity	specificity				
		100	75		100	75		100	100				

Receiver operating characteristics for T_{sprue} and T_{c-max}, using a 4.5°C the variables is given below.
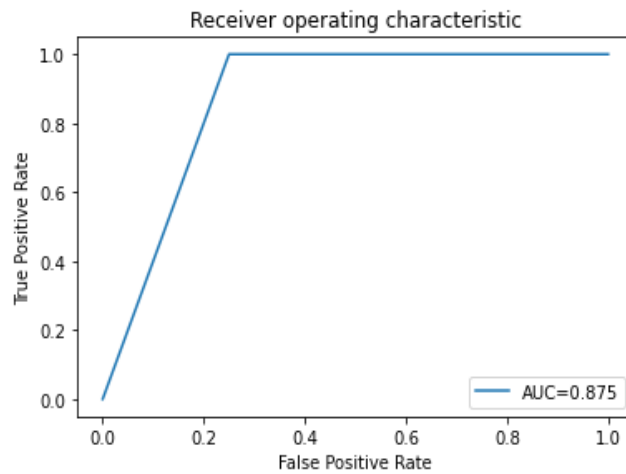
REFERENCES

Ayylldlz, S., Dursun, A. M., Ylldlrlm, V., Ince, M. E., Gülçelik, M. A. and Erdöl, C. (2020) '3D-Printed Splitter for Use of a Single Ventilator on Multiple Patients during COVID-19', *3D Printing and Additive Manufacturing,* 7(4), pp. 181-185.

Bagalkot, A., Pons, D., Clucas, D. and Symons, D. (2019) 'A methodology for setting the injection moulding process parameters for polymer rapid tooling inserts', *Rapid Prototyping Journal,* 25(9), pp. 1493-1505.

Baruffi, F., Calaon, M. and Tosello, G. (2018) 'Micro-Injection Moulding In-Line Quality Assurance Based on Product and Process Fingerprints', *Micromachines,* 9(6), pp. 293.

Bibber, D. (2012) 'Secrets of success in micro molding', *Plastics Technology,* 58(3), pp. 33-37+97.

Bibber, D. (2014) 'Micro molding thin-walled devices', *Manufacturing Engineering,* 152(4), pp. 35-37.

Boinski, A. K., Riemer, O., Karpuschewski, B., Schneider, M., Guttmann, M. and Worgull, M. (2022) 'Fast tool machining and hot embossing for the manufacture of diffractive structured surfaces', *Precision Engineering,* 74, pp. 12-19.

Dilag, J., Chen, T., Li, S. and Bateman, S. A. (2019) 'Design and direct additive manufacturing of three-dimensional surface micro-structures using material jetting technologies', *Additive Manufacturing,* 27, pp. 167-174.

Formlabs (2022) *How to Estimate Injection Molding Cost?* Available at: https://formlabs.com/uk/blog/injection-molding-cost/ (Accessed: 17.05.2022).

Gohn, A. M., Brown, D., Mendis, G., Forster, S., Rudd, N. and Giles, M. (2022) 'Mold inserts for injection molding prototype applications fabricated via material extrusion additive manufacturing', *Additive Manufacturing,* 51, pp. 102595.

Griffiths, C. A., Dimov, S. S., Scholz, S. G., Tosello, G. and Rees, A. (2014) 'Influence of injection and cavity pressure on the demoulding force in micro-injection moulding', *Journal of Manufacturing Science and Engineering, Transactions of the ASME,* 136(3).

Gulcur, M. (2019) *Process Fingerprinting of Microneedle Manufacturing Using Conventional and Ultrasonic Micro-injection Moulding.* [Online] Available at: http://hdl.handle.net/10454/19048 (Accessed: 2022-07-06t09:15:00z).

Gülçür, M., Brown, E., Gough, T., Romano, J.-M., Penchev, P., Dimov, S. and Whiteside, B. (2020) 'Ultrasonic micromoulding: Process characterisation using extensive in-line monitoring for micro-scaled products', *Journal of Manufacturing Processes,* 58, pp. 289-301.

Gülçür, M., Romano, J.-M., Penchev, P., Gough, T., Brown, E., Dimov, S. and Whiteside, B. (2021) 'A cost-effective process chain for thermoplastic microneedle manufacture combining laser micro-machining and micro-injection moulding', *CIRP Journal of Manufacturing Science and Technology,* 32, pp. 311-321.

Gülçür, M. and Whiteside, B. (2021) 'A study of micromanufacturing process fingerprints in micro-injection moulding for machine learning and Industry 4.0 applications', *International Journal of Advanced Manufacturing Technology,* 115(5-6), pp. 1943-1954.

Harris, R. A., Newlyn, H. A. and Dickens, P. M. 'Selection of mould design variables in direct stereolithography injection mould tooling'. *Proceedings of the Institution of Mechanical Engineers, Part B: Journal of Engineering Manufacture*, 499-505.

Harris, R. A., Newlyn, H. A., Hague, R. J. M. and Dickens, P. M. (2003) 'Part shrinkage anomilies from stereolithography injection mould tooling', *International Journal of Machine Tools and Manufacture,* 43(9), pp. 879-887.

Help Online - Origin Help - 30.1.104 Logistic (2022). Available at: https://www.originlab.com/doc/origin-help/logistic-fitfunc (Accessed: 16.05.2022).

Holthusen, A. K., Riemer, O., Schmütz, J. and Meier, A. (2017) 'Mold machining and injection molding of diffractive microstructures', *Journal of Manufacturing Processes,* 26, pp. 290-294.

Kovács, J. G., Szabó, F., Kovács, N. K., Suplicz, A., Zink, B., Tábi, T. and Hargitai, H. (2015) 'Thermal simulations and measurements for rapid tool inserts in injection molding applications', *Applied Thermal Engineering,* 85, pp. 44-51.

Krizsma, S., Kovács, N. K., Kovács, J. G. and Suplicz, A. (2021) 'In-situ monitoring of deformation in rapid prototyped injection molds', *Additive Manufacturing,* 42, pp. 102001.

Marhöfer, D. M., Tosello, G., Islam, A. and Hansen, H. N. (2016) 'Gate Design in Injection Molding of Microfluidic Components Using Process Simulations', *Journal of Micro and Nano-Manufacturing,* 4(2).

Measurement of Glass Transition Temperatures byDynamic Mechanical Analysis and Rheology (2022). Available at: https://www.tainstruments.com/pdf/literature/RH100.pdf (Accessed: 01.10.2022).

Mendible, G. A., Saleh, N., Barry, C. and Johnston, S. P. (2022) 'Mechanical properties and crystallinity of polypropylene injection molded in polyjet and aluminum tooling', *Rapid Prototyping Journal,* 28(4), pp. 686-694.

Middleton, B. J., Goodship, V., Dallmann, R. and Charmet, J. 'Low cost injection moulding strategies for the fabrication of microfluidic devices'. *22nd International Conference on Miniaturized Systems for Chemistry and Life Sciences, MicroTAS 2018*, 563-566.

Peixoto, C., Valentim, P. T., Sousa, P. C., Dias, D., Araújo, C., Pereira, D., Machado, C. F., Pontes, A. J., Santos, H. and Cruz, S. (2022) 'Injection molding of high-precision optical lenses: A review', *Precision Engineering,* 76, pp. 29-51.

Romano, J. M., Gulcur, M., Garcia-Giron, A., Martinez-Solanas, E., Whiteside, B. R. and Dimov, S. S. (2019) 'Mechanical durability of hydrophobic surfaces fabricated by injection moulding of laser-induced textures', *Applied Surface Science,* 476, pp. 850-860.

Santoso, T., Syam, W. P., Darukumalli, S. and Leach, R. (2022) 'Development of a compact focus variation microscopy sensor for on-machine surface topography measurement', *Measurement: Journal of the International Measurement Confederation,* 187.

Stratasys (2022) *Vero: A Realistic, Multi-Color Prototypes in Less Time*. Available at: https://www.stratasys.com/en/materials/materials-catalog/polyjet-materials/vero/ (Accessed: 07.11.2021).

University of Bradford begins mass production of face shields for health service (2020). Available at: https://www.youtube.com/watch?v=hIZOQO9gWx8&ab_channel=UniversityofBradford (Accessed: 01.04.2022).

Ventilators, visors, volunteers and testing - more than a dozen more ways Warwick staff & students are helping respond to the pandemic (2020). Available at: https://warwick.ac.uk/newsandevents/pressreleases/ventilators_visors_volunteers/ (Accessed: 01.04.2022 2022).

Whiteside, B. R., Martyn, M. T., Coates, P. D., Allan, P. S., Hornsby, P. R. and Greenway, G. (2003) 'Micromoulding: Process characteristics and product properties', *Plastics, Rubber and Composites,* 32(6), pp. 231-239.

Whiteside, B. R., Martyn, M. T., Coates, P. D., Greenway, G., Allen, P. and Hornsby, P. 'Micromoulding: Process measurements, product morphology and properties'. *Plastics, Rubber and Composites*, 11-17.

Whiteside, B. R., Spares, R., Howell, K., Martyn, M. T. and Coates, P. D. (2005) 'Micromoulding: Extreme process monitoring and inline product assessment', *Plastics, Rubber and Composites,* 34(9), pp. 380-386.

Williams, M. A. and Kochhar, A. K. (2000) 'New product introduction practices in the British manufacturing industry', *Proceedings of the Institution of Mechanical Engineers, Part B: Journal of Engineering Manufacture,* 214(10), pp. 853-863.

Xu, X., Wang, L., Fratini, L., Ragai, I. and Nee, A. Y. C. (2021) 'Smart and resilient manufacturing in the wake of COVID-19', *Journal of Manufacturing Systems,* 60, pp. 707-708.

Yang, H., Lim, J. C., Liu, Y., Qi, X., Yap, Y. L., Dikshit, V., Yeong, W. Y. and Wei, J. (2017) 'Performance evaluation of ProJet multi-material jetting 3D printer', *Virtual and Physical Prototyping,* 12(1), pp. 95-103.

Zhang, H.-Y., Zhang, N., Han, W., Zhang, H.-G., Gilchrist, M. D. and Fang, F.-Z. (2021) 'Characterization of process and machine dynamics on the precision replication of microlens arrays using microinjection moulding', *Advances in Manufacturing,* 9(3), pp. 319-341.

Zhang, Y., Pedersen, D. B., Gøtje, A. S., Mischkot, M. and Tosello, G. (2017) 'A Soft Tooling process chain employing Additive Manufacturing for injection molding of a 3D component with micro pillars', *Journal of Manufacturing Processes,* 27, pp. 138-144.

Zhang, Y., Shan, S., Frumosu, F. D., Calaon, M., Yang, W., Liu, Y. and Hansen, H. N. (2022) 'Automated vision-based inspection of mould and part quality in soft tooling injection moulding using imaging and deep learning', *CIRP Annals,* 71(1), pp. 429-432.

Zhu, Y., Tang, T., Zhao, S., Joralmon, D., Poit, Z., Ahire, B., Keshav, S., Raje, A. R., Blair, J., Zhang, Z. and Li, X. (2022) 'Recent advancements and applications in 3D printing of functional optics', *Additive Manufacturing,* 52, pp. 102682.